

Alexandra Pulwicki
December 14, 2016

Results Basin Scale

Overview

This is a document that shows the sampled and full ranges of topographic parameters and then goes into the multiple linear regression and Bayesian model averaging that was used to explain SWE with topographic parameters.

Contents

1	Topographic parameters of study sites	2
1.1	Creating DEM	2
1.2	Calculating topographic parameters	4
1.3	Topographic parameters from QGIS to Matlab	8
1.4	Parameter correlation	9
1.5	Maps of topographic parameters and range of parameters sampled	9
2	Linear Regressions	21
2.1	Multiple Linear Regression	21
2.1.1	Background	21
2.1.2	Methods	22
2.1.3	Results	23
2.2	Bayesian Model Averaging	27
2.2.1	Background	27
2.2.2	Methods	29
2.2.3	Results	30
2.3	MLR and BMS comparison	34

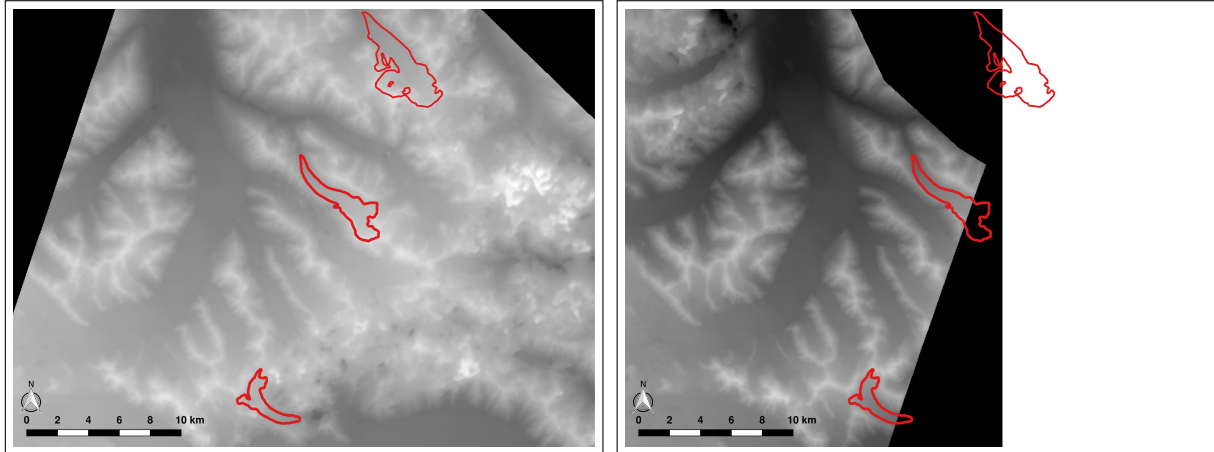
1 Topographic parameters of study sites

1.1 Creating DEM

Topographic parameters can be derived from a digital elevation model (DEM) of the study area. The DEM used in this project was created from imagery taken with the SPOT-5 satellite and it was provided at no cost by the French Space Agency (CNES) through the SPIRIT International Polar Year project (Korona and others, 2009). The DEM has a cell size of 40×40 m and the v2 version of the DEM, which employs a set of correlation parameters fit for steeper slopes (E. Berthier personal communication, 2016), was used.

Two DEMs were available for the Donjek Range. The first DEM (GES 08-029) was collected on September 3, 2007 and the second DEM (GES 07-044) was collected on September 13, 2007. Since the DEMs were collected in September, the surface would likely be at a seasonal minimum with minimum snow cover. This means that the surface described by the DEM represents the topography below the snow, which means that this study is similar in nature to other snow science investigations that examine ice free basins. A major flaw in using this DEM is that the DEM is from 2007 and almost certainly there have been changes in the end-of-summer glacier surface. However, the SPOT-5 DEM is currently the best resolution and most current DEM available for the study area.

and covered all three study glaciers (see Figure 1a) but a large part of Glacier 4 and some areas of Glacier 2 were masked by clouds and/or has limited contrast in the original stereo image pairs, resulting in incorrect elevation data (E. Berthier personal communication, 2016). The cloudy areas appear as a black regions on the DEM mask (not shown) and as distortion in the DEM, as seen in eastern area of Figure 1a. The second DEM (GES 07-044) spans only part of the Donjek Range, covering most of Glacier 4 and a large portion of Glacier 2 (see Figure 1b). This DEM had no cloud cover over Glacier 2 and 4. It was decided to merge the two DEMs to create a cloud free DEM that spanned all three glaciers.

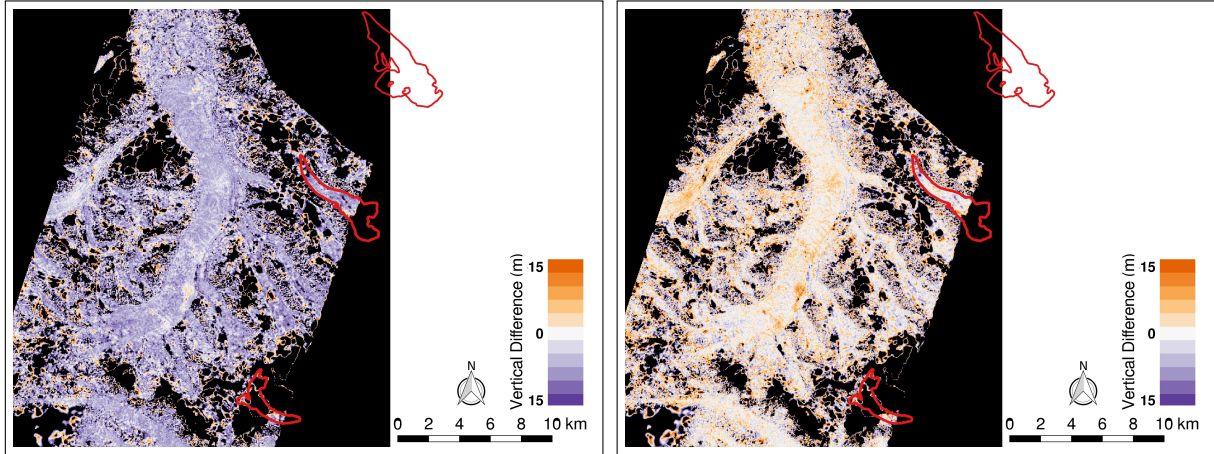


(a) DEM collected on September 3, 2007 (GES 08-029).

(b) DEM collected on September 13, 2007 (GES 07-044).

Figure 1: SPOT-5 DEMs available for the Donjek Range. Study glaciers are shown as red outlines. Areas with cloud cover have a distorted DEM as seen on the eastern side of (a).

The merging process was complicated by the fact that there was a horizontal and vertical discrepancy between the two DEMs. The second DEM had generally higher elevation values, as can be seen by the difference map shown in Figure 2a. Although the discrepancy was not consistent throughout the study area, the second DEM was generally higher than the first, as can be seen by the overall purple colour in Figure 2a.



(a) Difference between original DEMs

(b) Difference between corrected DEMs.

Figure 2: Vertical difference between DEMs in overlapping area. Difference was found by subtracting GES 08-029 from GES 07-044.

The discrepancy was corrected by E. Bertier (2016, personal communication) following an iterative 3D-coregistration algorithm presented in Berthier and others (2007). The

GES 07-044 DEM was arbitrarily chosen to be used as the reference DEM. Since there are no accurate ground control points and cells encompass an area with an elevation distribution, there was no way for us to determine whether one DEM was more accurate than the other. Further, the absolute value of the elevation is not necessarily important for the topographic regression, as long as the relative elevations are correct and that they represent the elevation profiles of the glacier. The reference DEM was first shifted vertically by +5.4 m, estimated using ICESat data (Bertier and others, 2010). Then, the mean horizontal and vertical (X, Y, Z) shift between the reference DEM and the GES 08-029 DEM was found by minimizing the standard deviation of the elevation difference between the DEMs. The values of the shift were ~2 m east, ~4 m north, and ~1.9 m vertically. The DEM was then reprojected in the same projection as the reference DEM.

Merging of the corrected DEMs

was completed in QGIS. First, the rasters were cropped to overlap by a few cells. The crop line was chosen by hand to include as much of the reference DEM as possible (fewer areas of poor data) but was some distance from the edge of the DEM, which can be distorted (see Figure 3). The second DEM was cropped to follow the same merge line but overlap with the first image by a few cells. This was done to avoid gaps in cell values that arise from cropping across a DEM cell. The merging was completed using the built in QGIS tool ‘Merge’.

The final DEM used for subsequent analysis can be seen in Figure ???. The contour lines (10 m) also plotted on this figure show sharp topographic gradients that are aligned with the merge line. Despite the corrections, there were still discrepancies along the intersection of the DEMs. However, these discrepancies were not present on the study glaciers and located more than 250 m from the edge of the glacier so this DEM was used as the final version for the Donjek Range. All subsequent topographic analysis and calculations was based on elevation taken from this DEM.

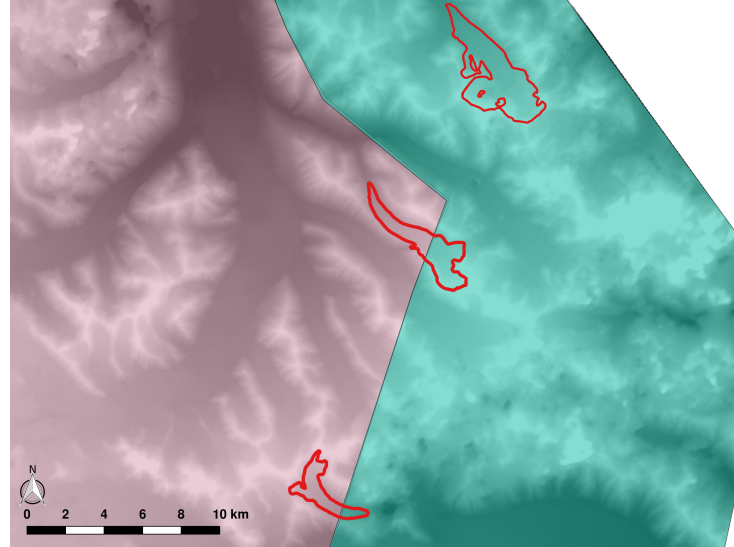


Figure 3: Outlines of the cropped GES 07-044 DEM (pink) and cropped GES 08-029 DEM (blue) used for merging. Note the small overlap of the two DEMs.

1.2 Calculating topographic parameters

Topographic parameters are used to describe local topography that affects snow distribution and act as proxies for physical processes that determine snow deposition and redistribution. Topographic parameters used in snow accumulation studies on glaciers include elevation (z), distance from centreline (d_C), slope (m), tangential (κ_T) and profile (κ_P)

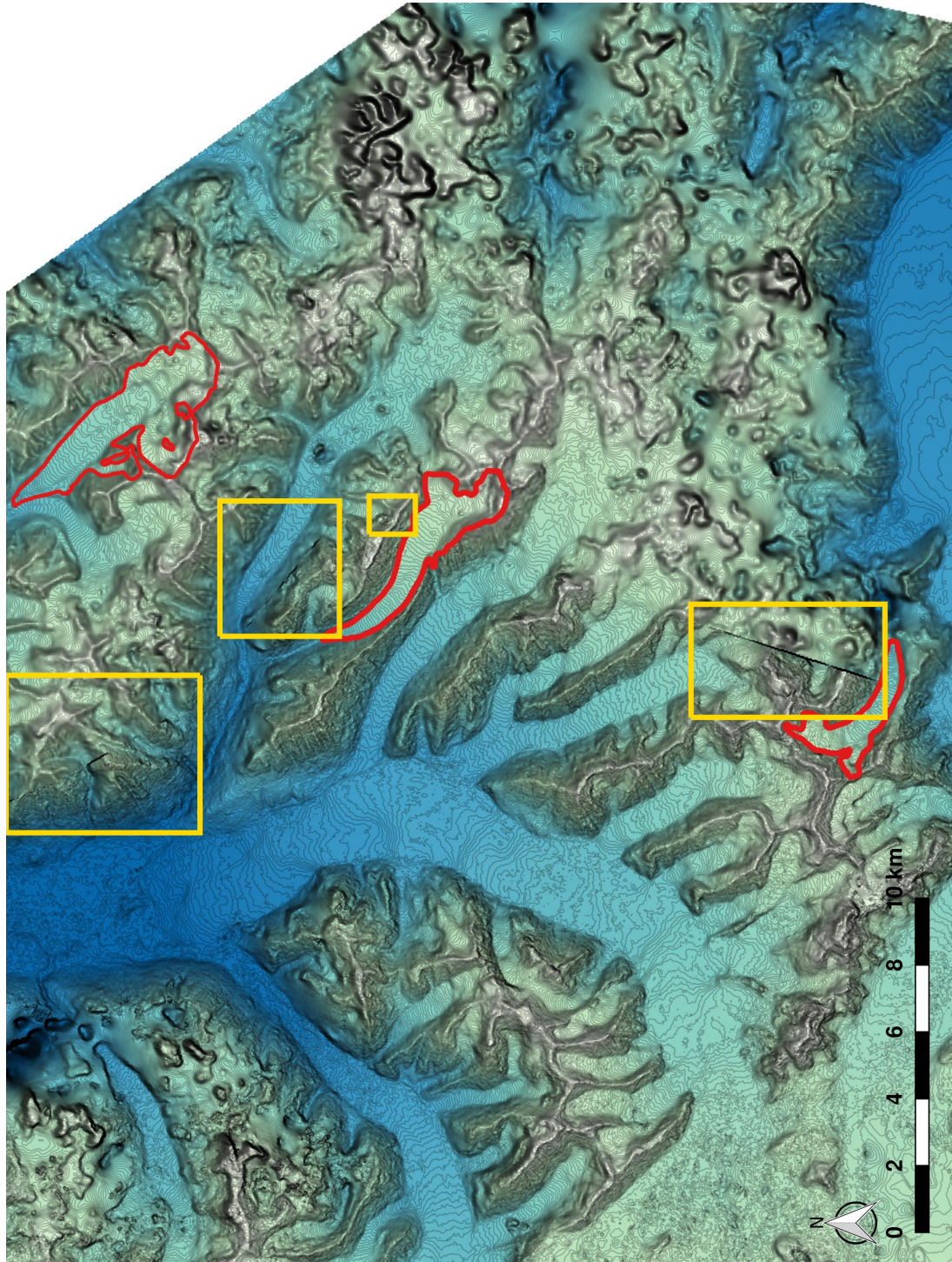


Figure 4: Merged DEM of the Donjek range from two corrected SPOT-5 DEMs with 10 m contour lines. Study glaciers are shown in red. Discrepancies between the DEMs along the merge line can be seen as linear features in the contour lines (appear as sharp topographic boundary) and are emphasized by the yellow boxes. Distorted contours in the eastern regions are a result of errors in the DEM.

curvature, “northness” (N), aspect (α), and Sx , which is a proxy for wind redistribution (Basist and others, 1994; Revuelto and others, 2014; McGrath and others, 2015).

A number of programs were used calculate topographic parameters from the SPOT-5 DEM. Distance from centreline and “northness” were calculated in Matlab. Sx was determined using a executable obtained from Adam Winstral that follows the procedure outlined in Winstral and others (2002). The remaining parameters were calculated using the `r.slope.aspect` module in GRASS GIS software run through QGIS as defined in Mitášová and Hofierka (1993) and described in Hofierka and others (2009).

The GRASS module implements a local polynomial approximation method of the form

$$z(x, y) = a \cdot x^2 + b \cdot y^2 + c \cdot x \cdot y + d \cdot x + e \cdot y + f. \quad (1)$$

This polynomial is fitted to 9 grid points (3×3 array) and the coefficients are determined by weighted least squares. First order partial derivatives are derived using Horn’s formula (Horn, 1981; Neteler and Mitášová, 2013). The gradient can be expressed as

$$\nabla \bar{z} = \left(\frac{\partial z}{\partial x}, \frac{\partial z}{\partial y} \right) = (2 \cdot a \cdot x + c \cdot y + d, 2 \cdot b \cdot y + c \cdot x + e). \quad (2)$$

Since we are interested in the value of the centre cell ($x = y = 0$), the gradient is simply

$$\nabla \bar{z} = (f_x, f_y) = (d, e), \quad (3)$$

where d and e are given by

$$f_x = \frac{(z_7 - z_9) + (2z_4 - 2z_6) + (z_1 - z_3)}{8 \cdot \Delta x}, \quad (4)$$

$$f_y = \frac{(z_7 - z_1) + (2z_8 - 2z_2) + (z_9 - z_3)}{8 \cdot \Delta y}. \quad (5)$$

Here, z_k refers to one of the grid cells surrounding the cell of interest, which is located at row i and column j of the DEM. So $z_3 = z_{i+1,j+1}$, $z_7 = z_{i-1,j-1}$, and so on. Δx and Δy are the grid spacing (resolution) of the DEM. The second order partial derivatives can be written as (Hofierka and others, 2009; Neteler and Mitášová, 2013)

$$f_{xx} = \frac{z_1 - 2z_2 + z_3 + 4z_4 - 8z_5 + 4z_6 + z_7 - 2z_8 + z_9}{6 \cdot (\Delta x)^2}, \quad (6)$$

$$f_{yy} = \frac{z_1 - 4z_2 + z_3 - 2z_4 - 8z_5 - 2z_6 + z_7 + 4z_8 + z_9}{6 \cdot (\Delta y)^2}, \quad (7)$$

$$f_{xy} = \frac{(z_7 - z_9) - (z_1 - z_3)}{4 \cdot \Delta x \Delta y}. \quad (8)$$

The second derivatives are most commonly used to calculate the curvature of a surface. The curvature at a given point on a curve is determined by finding the inverse of the radius of a circle that best fits the curve (Olaya, 2009). Convex surfaces have positive curvature and concave surfaces have negative curvature.

The calculation of topographic parameters is described below.

Elevation values were taken from the SPOT-5 DEMs directly.

Distance from centreline was calculated as the minimum distance between the Easting and Northing of the northwest corner of each cell and a centreline that was drawn by hand in QGIS. This was completed in Matlab using the script ‘CentrelineDistance.m’.

Slope is taken to be the steepest slope angle and is the magnitude of gradient (Mitášová and Hofierka, 1993). Using the gradient, it can be expressed as (Olaya, 2009)

$$m = \arctan(|\nabla \bar{z}|) = \arctan \left(\sqrt{(f_x)^2 + (f_y)^2} \right) \quad (9)$$

Tangential Curvature (horizontal curvature) represents the curvature in the direction of the contour tangent. The equation for tangential curvature can be written as (Olaya, 2009)

$$\kappa_T = -\frac{e^2 \cdot r - 2 \cdot d \cdot e \cdot s + d^2 \cdot t}{(d^2 + e^2) \cdot \sqrt{1 + d^2 + e^2}} \quad (10)$$

where d and e are as above and

$$r = \frac{\partial^2 z}{\partial x^2} = \frac{z_1 + z_3 + z_4 + z_6 + z_7 + z_9 - 2 \cdot (z_2 + z_5 + z_8)}{3 \cdot \Delta s^2} \quad (11)$$

$$s = \frac{\partial^2 z}{\partial x \partial y} = \frac{z_3 + z_7 - z_1 - z_9}{4 \cdot \Delta s^2} \quad (12)$$

$$t = \frac{\partial^2 z}{\partial y^2} = \frac{z_1 + z_2 + z_3 + z_7 + z_8 + z_9 - 2 \cdot (z_4 + z_5 + z_6)}{3 \cdot \Delta s^2} \quad (13)$$

Profile Curvature (vertical curvature) represents the curvature in the direction of the steepest slope (gradient). The equation for profile curvature can be written as (Olaya, 2009)

$$\kappa_P = -\frac{d^2 \cdot r + 2 \cdot d \cdot e \cdot r \cdot s + e^2 \cdot t}{(d^2 + e^2) \cdot \sqrt{(1 + d^2 + e^2)^3}} \quad (14)$$

“**Northness**” is a solar radiation parameter that has been shown to become increasingly important during the spring (Revuelto and others, 2014). It is also likely that this parameter may be related to sun included snow metamorphosis and/or sun crusts, both of which affect SWE and snow redistribution (McGrath and others, 2015). “Northness” is defined as the product of the cosine of aspect and sine of slope (Molotch and others, 2005). A value of -1 represents a steep, south facing slope, a value of +1 represents a steep, north facing slope, and a flat surfaces yield 0.

Aspect represent the orientation of the steepest slope, with 0° defined as north and no value given to cells that have no gradient. Using the gradient, it can be expressed

as (Olaya, 2009)

$$\alpha = 180 - \arctan\left(\frac{f_y}{f_x}\right) + 90 \cdot \frac{f_x}{|f_x|} \quad (15)$$

Sx represents wind exposure/shelter and is based on selecting a cell within a certain angle and distance from the cell of interest that has the greatest upward slope relative to the cell of interest (Winstral and others, 2002). This can be referred to as the maximum upwind slope. Negative Sx values represent exposure relative to the shelter-defining pixel, which means that the cell of interest was higher than the cell with greatest upward slope. Conversely, positive values represent sheltered cells. To determine Sx values, we use the equation

$$Sx_{A,dmax}(x_i, y_i) = \max \left[\tan^{-1} \left(\frac{z(x_v, y_v) - z(x_i, y_i)}{[(x_v - x_i)^2 + (y_v - y_i)^2]^{1/2}} \right) \right], \quad (16)$$

where A is the azimuth of the search direction, (x_i, y_i) are the coordinates of the cell of interest, and (x_v, y_v) are the set of all cell coordinates located along the search vector defined by (x_i, y_i) , the azimuth (A), and maximum search distance ($dmax$). Code for this calculation was provided by Adam Winstral (2016, personal communication). As done by McGrath and others (2015), we computed Sx at 5° azimuth increments for $dmax$ distances of 100, 200, and 300 m. These values were then correlated with observed values of SWE and the azimuth and $dmax$ values with the highest correlation were used for subsequent analysis (see Table 1). The code for calculating Sx requires a UTM raster formatted to ASCII in ArcGIS.

1.3 Topographic parameters from QGIS to Matlab

Table 1: Values of azimuth (A) and maximum search distance($dmax$), which define the Sx that had the highest correlation to observed SWE.

	A (° from North)	$dmax$ (m)	Correlation Coefficient
Glacier 4	85	300	-0.26
Glacier 2	330	300	0.56
Glacier 13	280	200	0.28

a .csv file and imported into Matlab with the script 'Import_Topo.m'. Note that selection of Sx values was completed first (see above) and only the Sx data with highest correlation to SWE was exported. After importing to Matlab, the sets of parameter values (x_i) were standardized (x_s) by $x_s = \frac{x_i - \mu}{\sigma}$. The resulting structure is called `topo_sampled` and is used in the MLR to be able to compare the explanatory power of each parameter (Section 2.1). A non-standardized copy of the topographic parameters at the sampling

The values of each topographic parameters at the sampling locations was determined in QGIS. The sampling locations were imported to QGIS and the Point Sampling Tool was used to determine the value of the cell of the raster for each topographic parameter at that location. This set of parameters that corresponded to each location was then exported to

locations was also kept for plotting purposes and is called `topo_sampled_ns`. Both structures are organized as a vector of values corresponding to the vectors in the `SWE` variable.

The raster data for each topographic parameter was also exported from QGIS as a `.csv` file and then imported into Matlab with the script '`Import_Topo.m`'. The values are stored in the structure `topo_full` and are a matrix, where each cell corresponds to one DEM cell. Cells outside of the glacier outline have no value (`NaN`).

1.4 Parameter correlation

The correlation between topographic parameters at sampling locations on each glacier is shown in Table 2. Correlation values were generally low, with the exception of the correlation between northness and aspect on Glacier 4 and northness and elevation on Glacier 2, which were both negative and larger than 0.7. Since there is little correlation and correlation that varies between glaciers, the use of a multiple linear regression with these topographic parameters as predictor variables is warranted.

1.5 Maps of topographic parameters and range of parameters sampled

Maps of the topographic parameters for each glacier are shown below. Additionally, the distribution of topographic parameter values and the sampled distribution for each parameter is also shown. The full range of parameters has highest frequencies for Glacier 13 and lowest for Glacier 4 because Glacier 13 is larger than Glacier 4. Frequency of sampled parameters are comparable between glaciers because the sampling schemes were similar.

Elevation maps in Figure 5 show higher elevations at the head of the glacier and lowest elevation at the terminus for all glaciers. Maximum elevation values are lower for Glacier 4 than the other two glaciers. The elevation distribution differs between glaciers. Glacier 4 and 13 have a larger number of mid-elevations (broader distribution) than Glacier 2 (sharp peaked distribution). The sampled distribution for all glaciers is markedly different than the full distribution as seen in Figure 6. In general, the distribution mean is lower and does not sample the full range of values. This is especially evident for Glacier 13 where a large portion of the higher elevations were not sampled. Unfortunately, high elevation locations are often dangerous to access and could not be sampled in situ.

Distance from centreline is shown in Figure 7. Note that Glacier 13 has two centrelines in the accumulation area because of the confluence of two major arms of the glacier. The sampled distribution generally matches the full distribution. This is likely because the hourglass sampling pattern allowed for locations across the whole width of the glacier to be measured, although this is generally limited to the ablation area. However, the sampling did not allow for the locations at a far distance from the centreline to be measured because these locations are generally in steep, inaccessible terrain.

Slope of the three study glaciers is shown in Figure 9. The majority of the area of the three glaciers has a slope of less than 20°, with only the margins of the accumulation

Table 2: Pearson correlation coefficients between topographic parameters at sampled locations. The parameters include aspect (α), elevation (z), northness (N), profile curvature (κ_P), slope (m), tangent curvature (κ_T), wind redistribution (Sx) and distance from centreline (d_C).

Glacier		α	z	N	κ_P	m	κ_T	Sx	d_C
Glacier 4	α	1	0.52	-0.78	0.24	-0.2	0.12	0.30	-0.12
	z	0	1	-0.53	0.16	<0.01	0.15	0.21	0.20
	N	0	0	1	-0.33	0.07	-0.13	-0.49	0.09
	κ_P	0	0	0	1	-0.20	0.44	-0.30	-0.16
	m	0	0	0	0	1	<0.01	0.20	0.36
	κ_T	0	0	0	0	0	1	-0.28	-0.01
	Sx	0	0	0	0	0	0	1	0.07
	d_C	0	0	0	0	0	0	0	1
	α	1	-0.02	0.04	0.13	-0.16	-0.02	-0.02	-0.12
Glacier 2	z	0	1	-0.62	0.06	-0.46	0.02	0.14	0.05
	N	0	0	1	-0.03	0.5	0.09	-0.15	0.32
	κ_P	0	0	0	1	-0.01	0.45	0.01	0.08
	m	0	0	0	0	1	-0.02	-0.07	0.12
	κ_T	0	0	0	0	0	1	-0.03	0.19
	Sx	0	0	0	0	0	0	1	-0.18
	d_C	0	0	0	0	0	0	0	1
	α	1	-0.24	-0.07	0.02	-0.1	0.02	0.08	0.06
	z	0	1	0.14	0.08	0.01	0.01	-0.24	0.13
Glacier 13	N	0	0	1	0.06	0.24	0.08	-0.01	0.07
	κ_P	0	0	0	1	-0.02	0.37	-0.04	0.07
	m	0	0	0	0	1	-0.15	-0.02	0.09
	κ_T	0	0	0	0	0	1	<0.01	<0.01
	Sx	0	0	0	0	0	0	1	-0.06
	d_C	0	0	0	0	0	0	0	1

area and a few steps on Glacier 13 have steep slopes. The distribution of slope is similar between glaciers (see Figure 10). All have a peak frequency around 10° and few area with very steep slopes. The sampled distribution matches the full distribution near this peak but severely under samples steep slope (due to dangerous conditions).

Tangential curvature is shown in Figure 11 and profile curvature is shown in Figure 13. The curvature values are generally moderate and centred about 0. The distribution of sampled curvature closely matches the full distribution although high curvature areas were not sampled (see Figure 12 and 14).

Aspect of the glacier surface is shown in Figure 15. Glacier 2 and 13 have similar aspect distributions, with a mean aspect of $\sim 100^\circ$. Glacier 4 has a mean aspect of $\sim 300^\circ$, which is roughly 180° to that of Glacier 2 and 13. The sampled distribution, as shown in Figure 16, for Glacier 4 follows that of the full distribution relatively well. However, the sampled distribution of Glacier 2 and 13 does not match that of the full distribution and there are many aspects that were not sampled.

“Northness” for all study glaciers is shown in Figure 17. The majority of cells have values close to zero, which is likely due to their low slope values. Even for Glacier 4, which is largely south facing and should thus have lower values of “northness”, has a distribution with a mean close to zero. The low slope values mean that the values of “northness” were determined largely by the aspect, which can be seen by the resemblance between the “northness” map and the aspect map.

Sx maps over the study glaciers are shown in Figure 19 and the wind direction and maximum search distance with the highest correlation to SWE for each glacier are shown in Table 1. For Glacier 4, an approximately east wind and 300 m search distance were most strongly correlated. The correlation was negative, which means that negative values of Sx (exposure) correspond to areas with larger SWE (more snow). This is counter intuitive and perhaps indicates that Sx is not an appropriate topographic parameter to correlate with SWE on Glacier 4. Despite this, Sx was retained in future analysis for consistency between glaciers. For Glacier 2, a north wind with a 300 m search distance was most strongly correlated and for for Glacier 13, a west wind with a 200 m search distance exhibited the strongest correlation. Both of these correlations were positive, so a more positive Sx value (sheltered) corresponded to higher values of SWE (more snow). The correlation values for Glacier 4 and 2 were low (<0.3), which indicates that Sx will likely be an insignificant in modelling snow accumulation. The correlation between Sx and SWE on Glacier 2 is relatively high (0.56).

Full distribution of Sx , as seen in Figure 20, is different for each glacier. Glacier 2 has a mean less than zero, indicating that a large portion of the glacier has exposed topography. Glacier 4 and 13 have positive mean values of Sx , indicating more sheltered topography. The sampled distribution for Glacier 4 and 2 generally follows that of the full distribution, although extreme values are not adequately sampled. For Glacier 13, the sample distribution does not closely match that of the full distribution, particularly for larger, more positive, values of Sx .

Overall, the sampled topographic parameters are representative of the full distribution of parameters. Extreme values are grossly under sampled so that the full range of parameter values was not sampled. This was largely do to dangerous travel conditions

and an inability to quickly and accurately measure snow depth in the accumulation area. As a result, extrapolation of regression models will likely result in large errors. This is especially relevant in the accumulation area, which has extreme values for all parameters. Errors in the accumulation area are especially important to acknowledge because this area has the most accumulation and is likely to skew final winter mass balance values. It is also important to note that for a number of parameters (especially elevation) the sampling distribution is off-set from that of the full distribution. Generally, the sampled values do not fully capture the variance in topographic parameters but a regression is still valuable to conduct since topographic regressions are common when estimating winter mass balance. Acknowledging that this methodology is limited and prone to extrapolation errors is paramount to capturing uncertainty in accumulation studies.

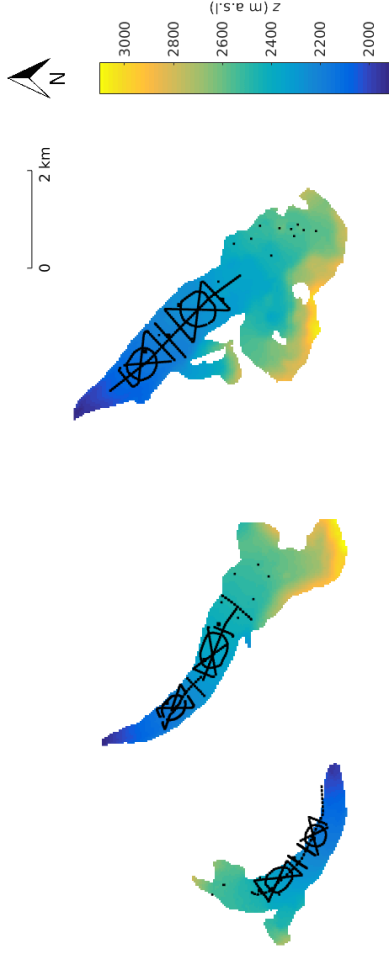


Figure 5: Values of elevation used in the topographic regressions for three study glaciers. This DEM is derived from a SPOT5 satellite image and has a grid size of 40x40 m. Subsequent topographic parameters were derived from this DEM.

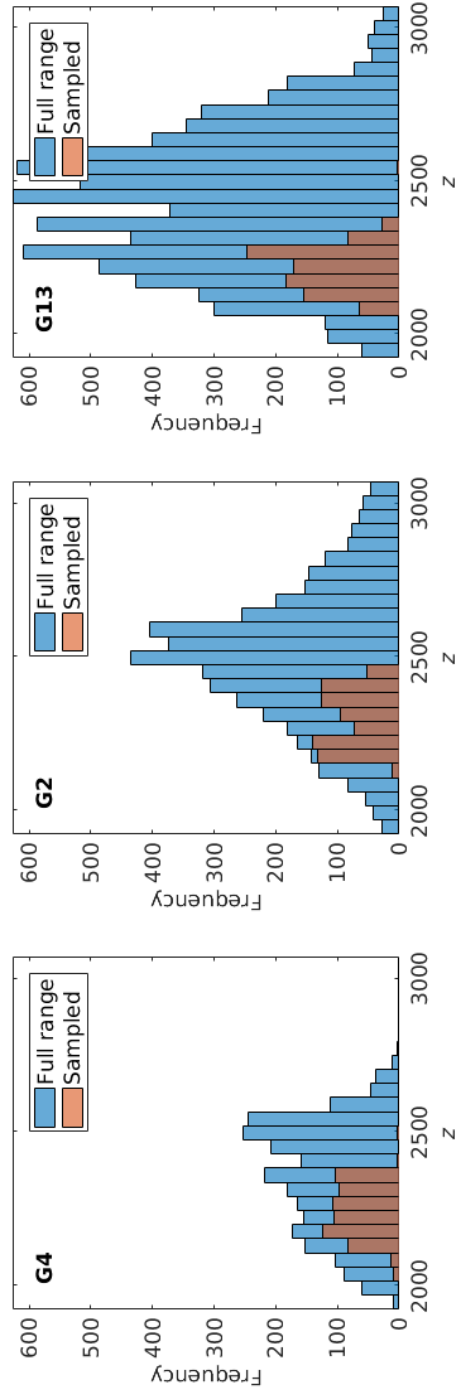


Figure 6: Range of elevation sampled as compared to total range of elevation of study glaciers.

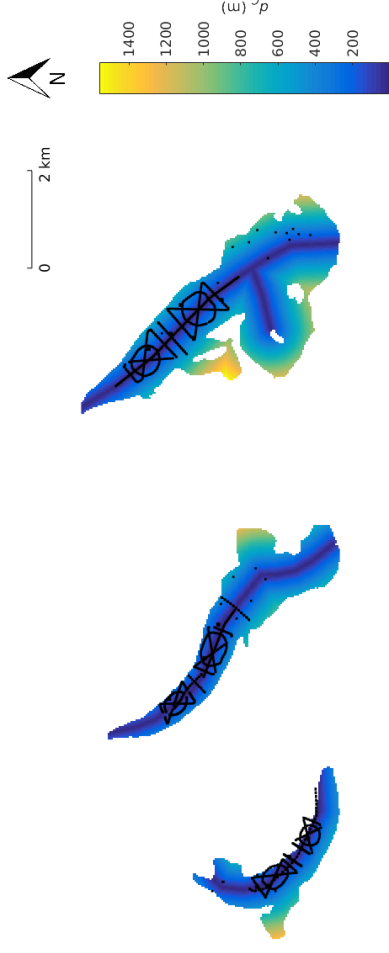


Figure 7: Values of distance from centreline used in the topographic regressions for three study glaciers. Centreline was drawn by hand in QGIS.

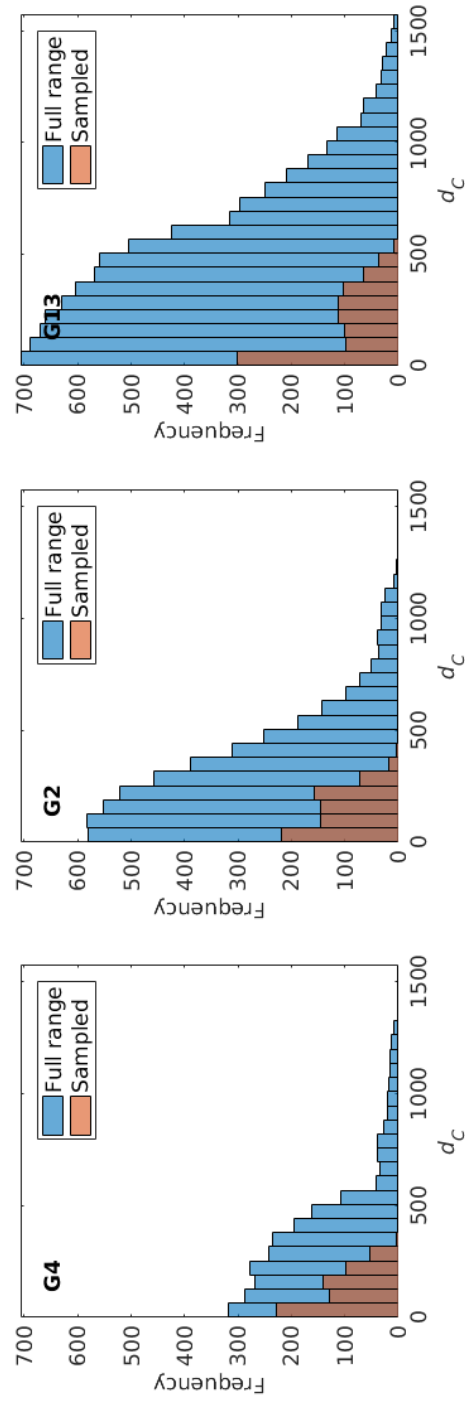


Figure 8: Range of distance from centreline sampled as compared to total range of distance from centreline of study glaciers.

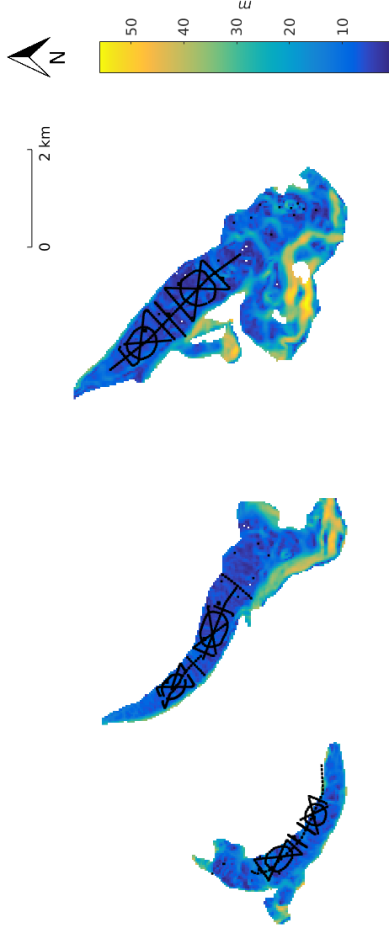


Figure 9: Values of slope used in the topographic regressions for three study glaciers. Values were derived from a SPOT5 satellite derived DEM (grid size of 40x40 m) in QGIS.

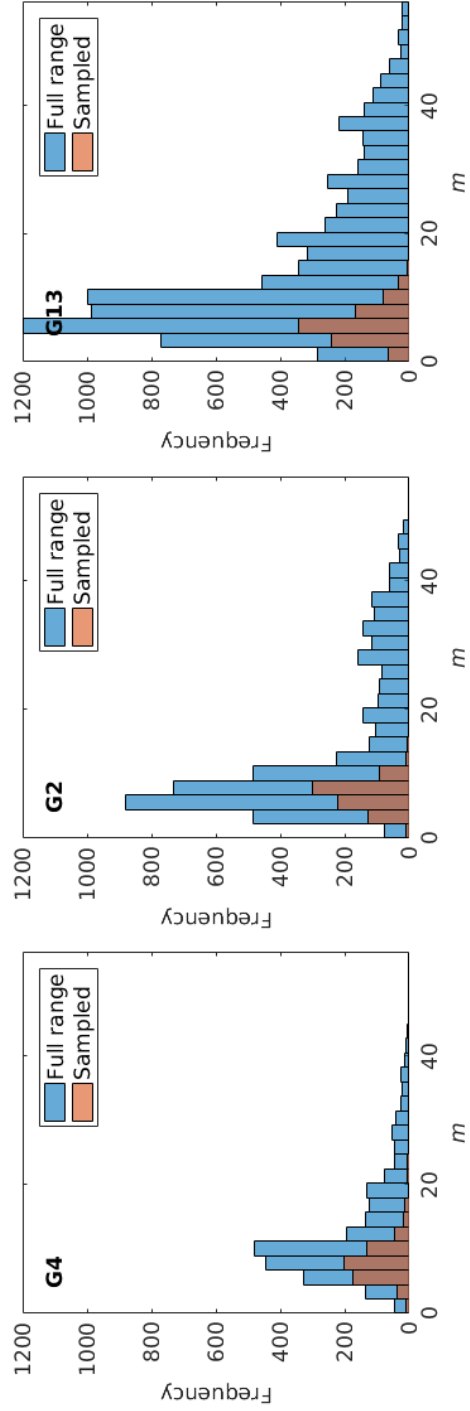


Figure 10: Range of slope sampled as compared to total range of slope of study glaciers.

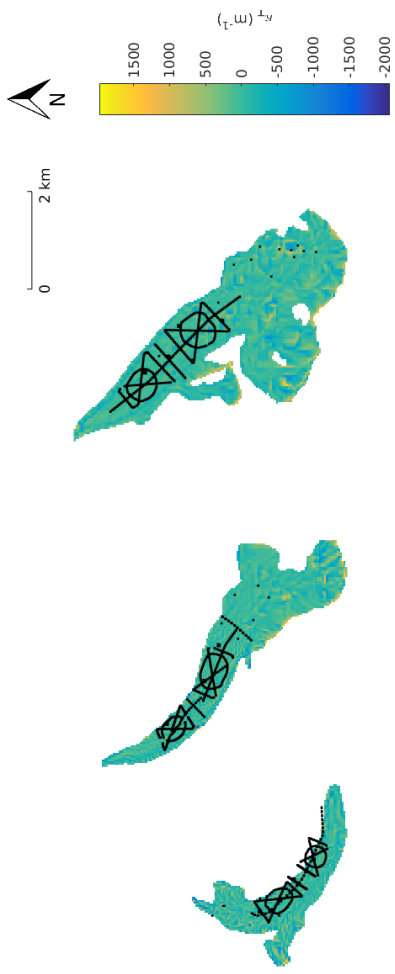


Figure 11: Values of tangential curvature used in the topographic regressions for three study glaciers. Values were derived from a SPOT5 satellite derived DEM (grid size of 40x40 m) in QGIS.

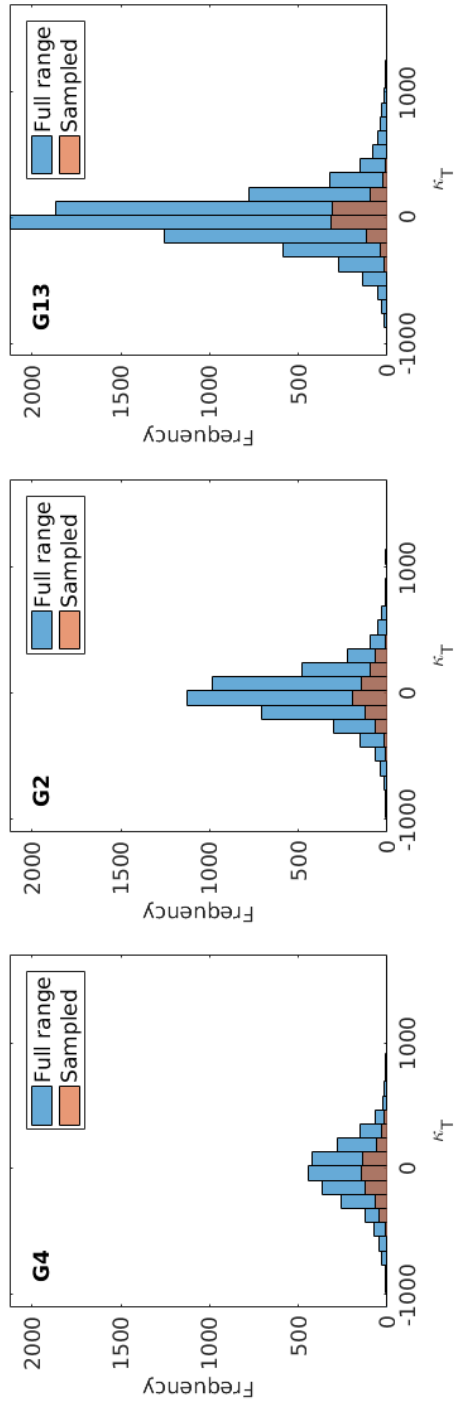


Figure 12: Range of tangential curvature sampled as compared to total range of tangential curvature of study glaciers.

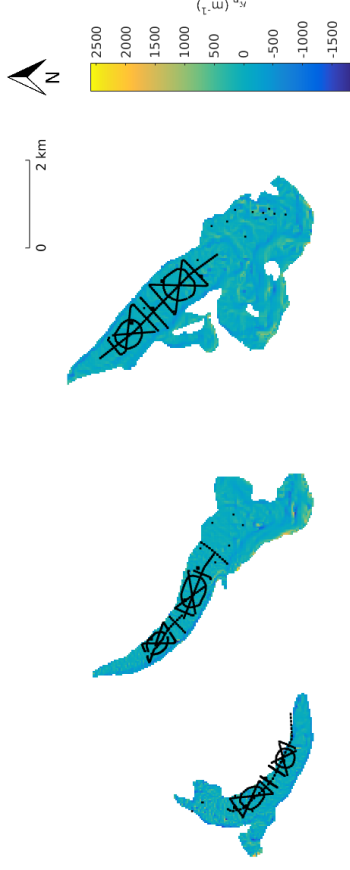


Figure 13: Values of distance from centreline used in the topographic regressions for three study glaciers. Values were derived from a SPOT5 satellite derived DEM (grid size of 40x40 m) in QGIS.

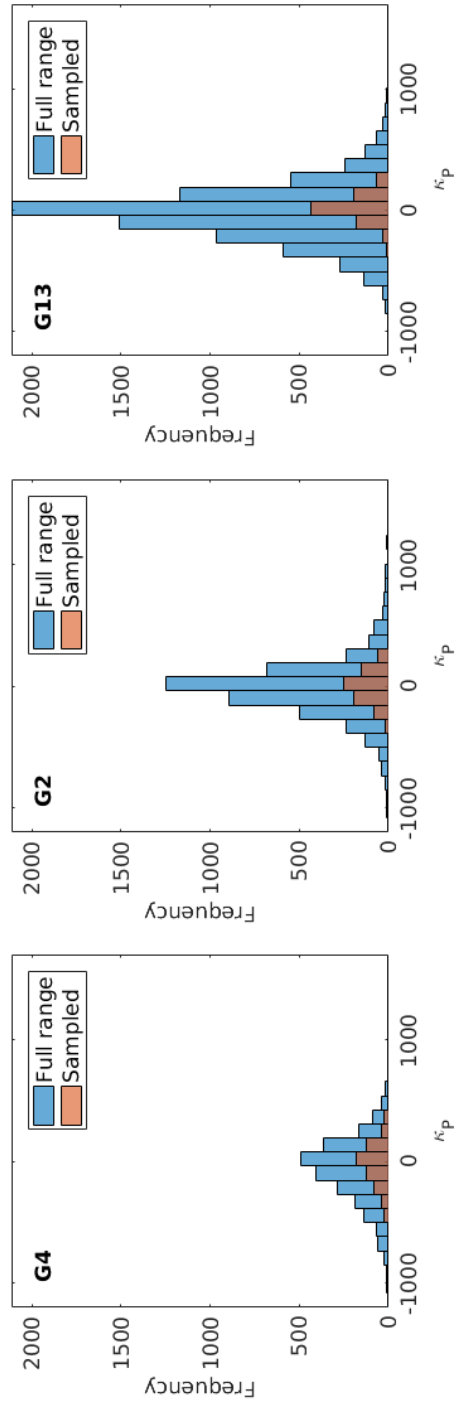


Figure 14: Range of profile curvature sampled as compared to total range of profile curvature of study glaciers.

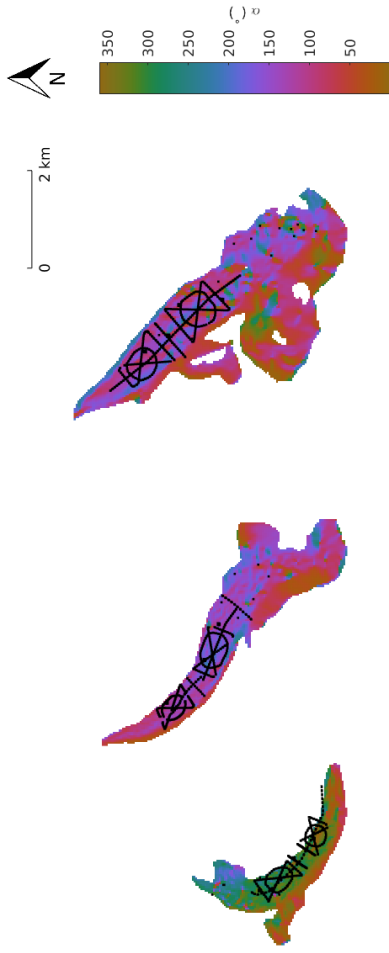


Figure 15: Values of aspect, which represent what direction a slope is facing (0° defined as north), used in the topographic regressions for three study glaciers.

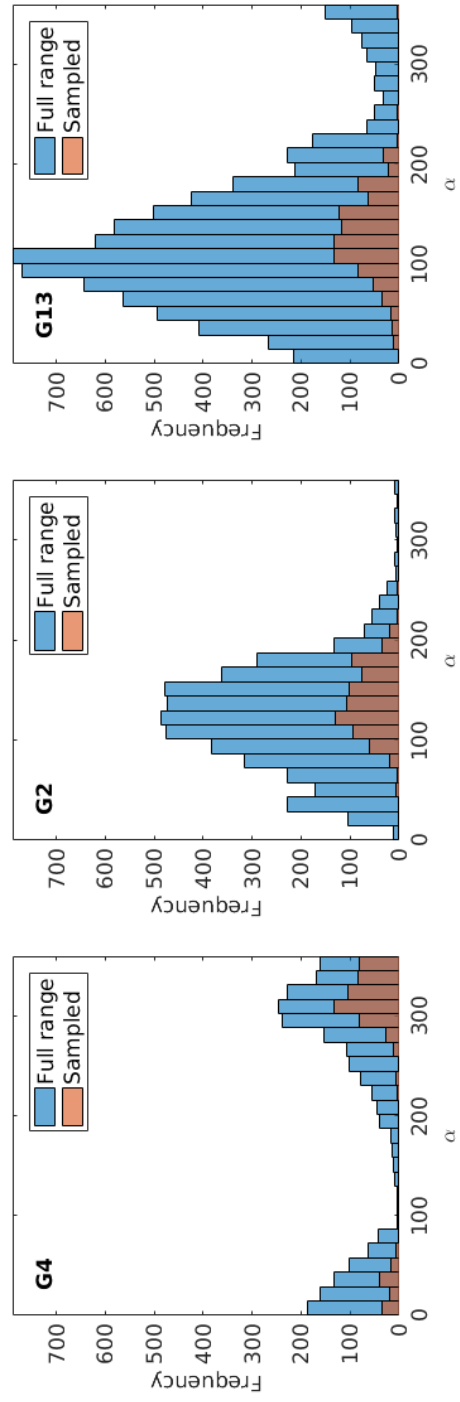


Figure 16: Range of aspect sampled as compared to total range of aspect of study glaciers.

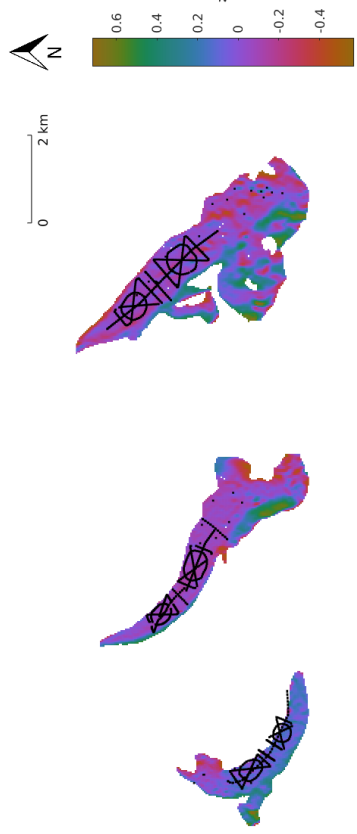


Figure 17: Values of “northness” used in the topographic regressions for three study glaciers. “Northness” is defined as the product of the cosine of aspect and sine of slope. A value of -1 represents a steep, south facing slope, a value of +1 represents a steep, north facing slope, and flat surfaces yield 0. Values were derived from a SPOT5 satellite derived DEM (grid size of 40x40 m) in QGIS.

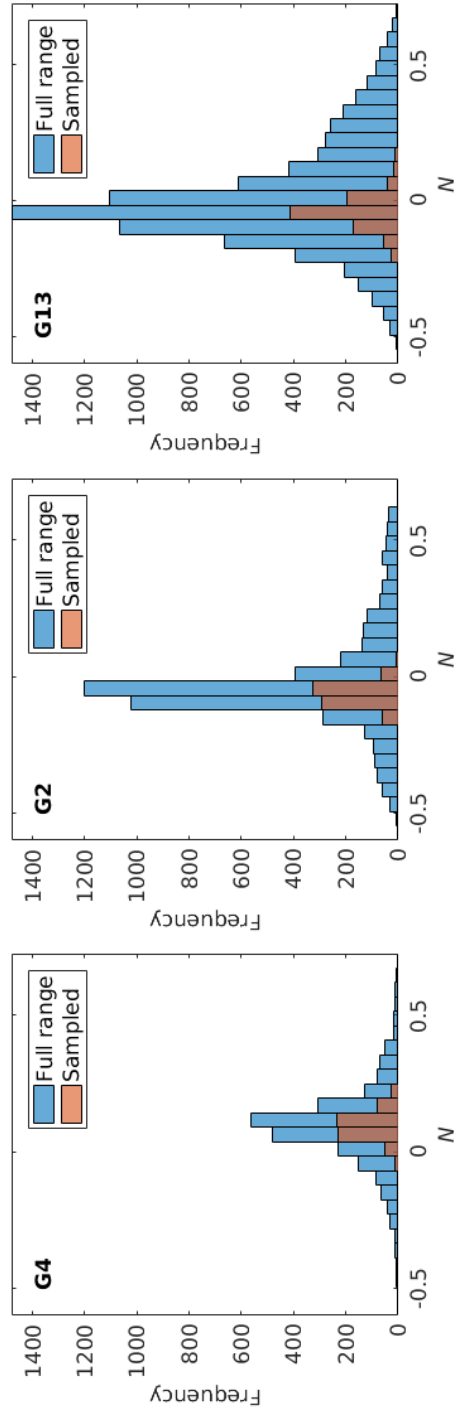


Figure 18: Range of “northness” sampled as compared to total range of “northness” of study glaciers.

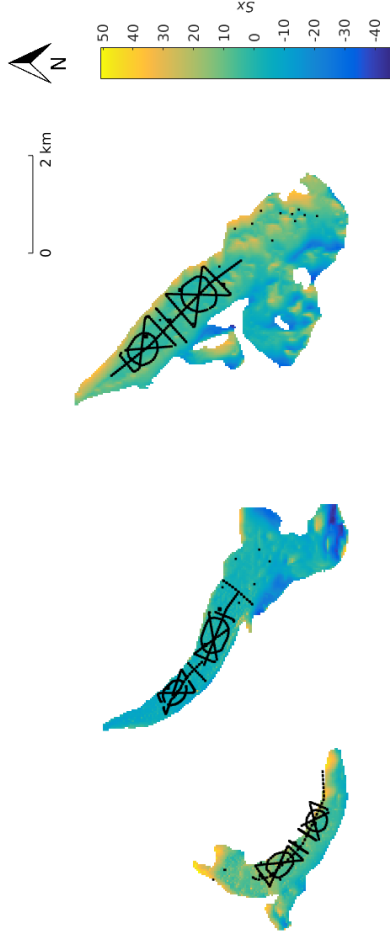


Figure 19: Values of S_x , which is a wind redistribution parameter, used in the topographic regressions for three study glaciers. See section ?? and the original paper by Winstral and others (2002) for more details on calculation. See Table 1 for values of best correlated azimuth and maximum search distance for each glacier.

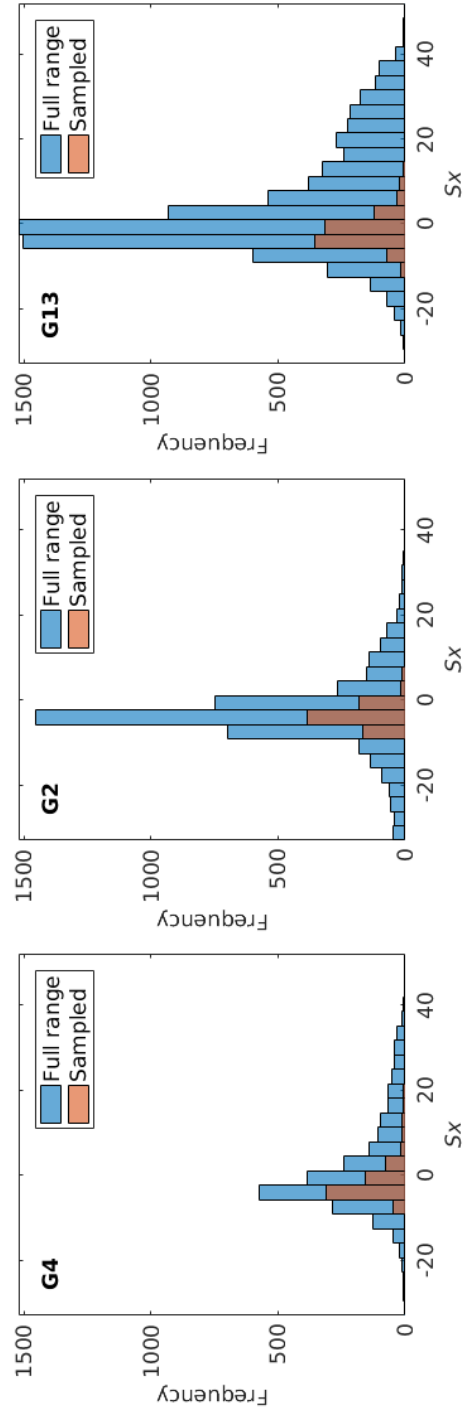


Figure 20: Range of S_x sampled as compared to total range of S_x of study glaciers.

2 Linear Regressions

Relating snow accumulation and terrain parameters to better predict accumulation within a basin has been employed for decades (e.g. Woo and Marsh, 1978; Molotch and others, 2005; McGrath and others, 2015). The most common type of relation between topographic parameters and accumulation is a linear regression, where the observed snow water equivalent (SWE) is related to a linear combination of topographic parameters at each measurement location.

A linear regression takes the form

$$\mathbf{y} = \mathbf{X}\boldsymbol{\beta} + \boldsymbol{\varepsilon}, \quad (17)$$

where the matrix \mathbf{X} contains the set of independent regressors \mathbf{x}_i used to explain the dependant variable \mathbf{y} (Davis and Sampson, 1986). The regression coefficients for each regressor is given by $\boldsymbol{\beta}$ and the error or noise of the system is given by $\boldsymbol{\varepsilon}$. Applied to this study, the matrix of independent regressors (\mathbf{X}) contains the topographic parameters at the sampling locations, the dependant variable \mathbf{y} contains the observed SWE, and the $\boldsymbol{\beta}$ values are determined using a fitting model. While there are many types of fitting models, the ones employed in this study are multiple linear regression (MLR) and Bayesian model averaging (BMA).

Once $\boldsymbol{\beta}$ values have been estimated, they can then be used to predict values of the dependant variable in other locations where regressors are known (Davis and Sampson, 1986). Known values of topographic parameters can be multiplied by their respective $\boldsymbol{\beta}$ coefficients and added together to obtain the modelled or predicted value of SWE for that DEM grid cell.

2.1 Multiple Linear Regression

2.1.1 Background

Perhaps the most basic and well used method for relating SWE and topographic parameters is a multiple linear regression (MLR) (e.g. Cohen and others, 2013). The best fit line of an MLR is the one described by coefficients that minimize the sum of squares of the vertical deviations of each data point from the line (Davis and Sampson, 1986). Note that if a point falls on the line then the deviation is zero and that the positive and negative deviations from the line do not cancel because the values are first squared and then summed. The residuals are simply the difference between the modelled and observed data.

To reduce the chance of over fitting the data, two additional methods were applied. The first method was model averaging over all possible models that allow for linear combinations of the chosen topographic parameters. An MLR was estimated for each model (total number of models is 2^n , where n is the number of topographic parameters) and the Bayesian information criterion (BIC) value was computed for the model according to

$$\text{BIC} = -2 \ln L(\hat{\theta}_k | y) + k \ln(n), \quad (18)$$

where the values of $\hat{\theta}_k$, which are the model parameters, maximizes the likelihood function for data y (Burnham and Anderson, 2004). The number of data points is n and the number of regressors is k . BIC values are used to assess the relative predictive success of models while penalizing for overfitting of data. While the absolute BIC value is meaningless, models can be selected or averaged using the relative BIC value, with lower values indicating a better model (Burnham and Anderson, 2004).

In this study, there was no reason to favour any of the models so a weighted average of all models based on their BIC values was conducted. The BIC values for each model (BIC_i) were used to determine the normalized weight of each model (w_i) relative to the best model (lowest BIC value BIC_{min}) according to (Burnham and Anderson, 2004)

$$w_i = \frac{e^{-0.5(BIC_i - BIC_{min})}}{\sum_{i=1}^R e^{-0.5(BIC_i - BIC_{min})}}. \quad (19)$$

When parameters were excluded from a model, a coefficient of zero was assigned to that parameter. The sum of the weighted coefficients gave the final β values.

The second method used to prevent over fitting was to calculate the MLRs within a cross validation framework. This meant that for each model, a randomly selected portion of the data was used to estimate regression coefficients and these were used to predict values that correspond to the remaining data (Kohavi and others, 1995). The root mean squared error (RMSE) between the modelled and observed data was then calculated. This process was done one thousand times and the set of coefficients that resulted in the lowest RMSE were then chosen for that model.

Together, cross validation allowed for reputable choosing of regression coefficients for each possible model and model averaging with BIC weights allowed for stability of final coefficient values and favouring of simpler models, which would help to identify main topographic drivers of snow accumulation.

2.1.2 Methods

A multiple linear regression (MLR) between snow water equivalent (SWE) and all linear combinations of the calculated topographic parameters was completed. This methodology for calculating the MLR also involved using cross validation, where a portion of the data is withheld from the MLR fit and these points are then used to assess the ability of the MLR to predict values. The MLR fit with the best prediction ability is then carried forward.

The MLR was completed with the following steps (executed using the function 'ML-Rcalval.m'):

1. The topographic parameters
2. The `topo_sampled` structure for one glacier as well as the `SWE` structure is passed into the function.
3. A set of initializations is completed. This includes 1) creating a logical matrix to choose all linear combination of topographic parameters, 2) selecting the number of

- runs, 3) creating a matrix of random numbers for selecting data point in the cross validation procedure, 4) initializing matrices, and 5) converting the input structure to a table.
4. For each linear combination of topographic parameters, one thousand runs of a cross validation MLR are then executed. Two-thirds of the total data is randomly selected (Kohavi and others, 1995) to use for calculating the regression (using the function `regress()` which is a basic regression function with fast execution). The MLR equations is used to predict the SWE using the remaining one-quarter of the topographic parameters. The root-mean-squared error (RMSE) between the predicted and observed SWE values is then calculated and the MLR equation with the lowest RMSE is then chosen for that combination of topographic parameters. The function `fitlm()` is then used to calculate the MLR from the set of data that gave the lowest RMSE. This function is slower but calculates a number of additional values that characterize the fit of the model. One of these values is the Bayesian information criterion (BIC), which allows for model selection among a finite set of models (Burnham and Anderson, 2004). The BIC from the best model for each combination of topographic parameters is saved.
 5. A weighted sum of all models found using linear combinations of topographic parameters was then found. The BIC values for each model (BIC_i) were used to determine the normalized weight of each model (w_i) relative to the best model (lowest BIC value BIC_{min}) according to Eq. 19.
 6. The percent variance ($var\%$) explained by each parameter was calculated using the equation $var\% = \frac{SSr}{SSt} \times 100$, where SSr is the sum of squares of the residual (fitted topographic parameters) and SSt is the total sum of squares (SWE observations). The final coefficients and the percent varience explained by each one can be found in the `coeffs_final` table within the function and in the `mlr` structure when run for all density options and glaciers in the main script 'TopoRegression.m'.
 7. The residuals of the fit have also been calculated as a separate variable than can be returned when the function is called. The residual was calculated as the difference between the predicted and observed value.

2.1.3 Results

The coefficients determined using MLR for density Option 8 can be seen in Table 3. These coefficients were found for standardized values of topographic parameters so their magnitude is indicative of their importance in predicting SWE. The range of percent variance explained by each variable (from all density options) can be seen in Figure ???. The fit between modelled SWE and observed SWE for each glacier for density Option 8 can be seen in Figure 21 and the fit for all density options in Figure 22. The distribution of residuals in then plotted in Figure 23. A map of the predicted values of SWE over the entire glacier using density option 8 can be seen in Figure ??.

For Glacier 4, the largest coefficients are distance from centreline and slope, which are an order of magnitude larger than the remaining coefficients. Both coefficients are nega-

tive, which indicates less snow along the margins of the glacier and less on steeper slopes. These coefficients account for the largest percentage of variance explained, although this percentage is very small (< 2% each). The map of predicted SWE for the entire glacier closely resembles the distribution of distance from centreline (Figure 7), which also shows its dependence on this parameter. Overall, the modelled winter balance for Glacier 4 is very poorly explained by the topographic parameters, which results in no correlation between modelled and observed SWE ($R^2 = 0.04$). The modelled values of SWE are largely determined by the intercept value. RMSE???

For Glacier 2, the largest coefficient (by an order of magnitude) is elevation. This coefficient is positive, which means that SWE will increase with elevation. Elevation explains the largest amount of variance (52%) and this is consistent for all density options. The map of modelled SWE shows this strong dependence on elevation since the values closely resemble the elevation map (Figure 5). Overall, the modelled winter balance is moderately good estimation of observed SWE ($R^2 = 0.57$) although it tends to underestimate the amount of accumulation.

For Glacier 13, the largest coefficient is elevation with distance from centreline and “northness” also of the same order of magnitude. All three coefficients are positive, which means that cell at higher elevation, closer to the margins, and more north facing had higher amounts of SWE. Elevation explains the majority of the variance (24%), while distance from centreline and “northness” explain far less (<3% each). The map of modelled SWE displays an increase with elevation, although it is not strong considering the large range of elevation on this glacier. Overall, the MLR modelled winter balance is poorly related to observed SWE ($R^2 = 0.3$) and tends to underestimate the amount of accumulation.

Qualitatively, there is little variation in the fit between modelled and observed winter balance between the various density options for all glaciers and the residuals display a similar distribution between the density options. The percent variance explained by each parameter also varies little between different density options.

Table 3: MLR coefficients for topographic regression between measured SWE and standardized topographic parameters that include distance from centreline (d_C), elevation (z), aspect (α), slope (m), northness (N), profile curvature (κ_P), tangent curvature (κ_T), and wind redistribution (Sx). Since parameters are standardizes, the magnitude of the coefficients is representative of their importance in predicting SWE. The root-mean-squared error (RMSE) between modelled SWE using those coefficients and observed SWE is also given.

	Glacier 4	Glacier 2	Glacier 13
d_C	-0.017	0.017	0.025
z	0.001	0.118	0.052
α	<0.001	-0.006	<0.001
m	-0.018	-0.002	-0.007
N	0.001	<0.001	0.015
κ_P	0.001	<0.001	-0.004
κ_T	<0.001	<0.001	-0.002
Sx	0.001	0.008	<0.001
Intercept	0.629	0.264	0.242
RMSE			

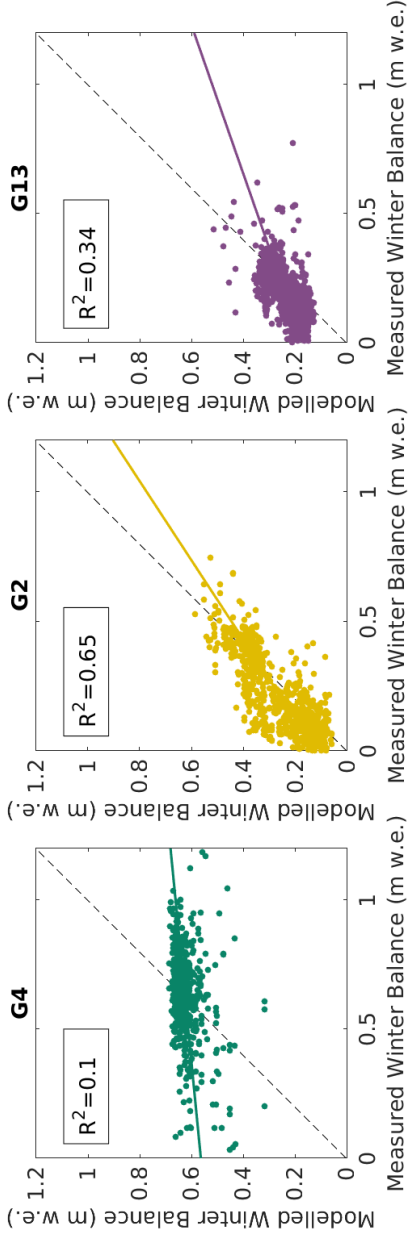


Figure 21: Comparison of predicted (MLR) and observed (original) snow water equivalent (SWE) for three study glaciers. The SWE values were calculated inverse distance weighted snowpit densities (Option 8).

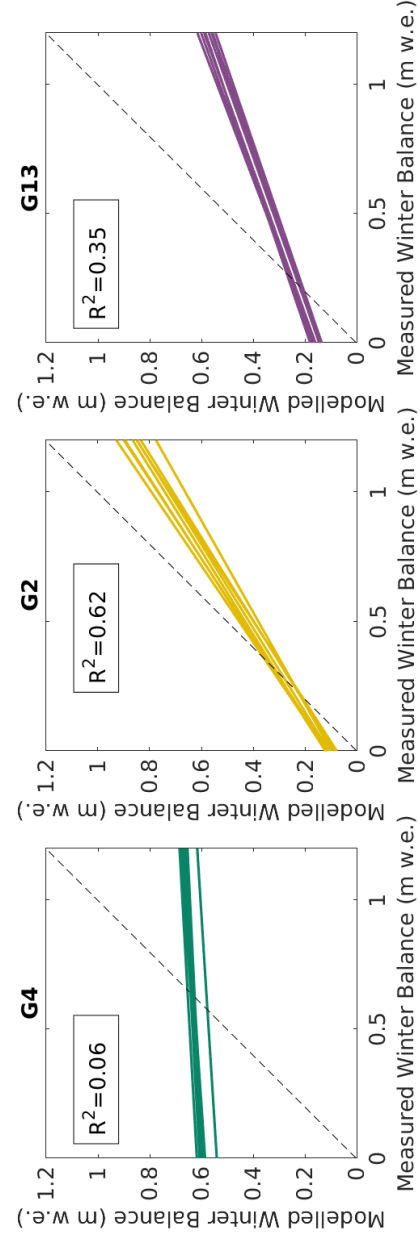


Figure 22: Plot of all linear fits between modelled and observed SWE using eight options for calculating density. Mean R^2 value is shown for each sub-plot and a reference 1:1 line is also provided. See Figure 21 for a plot of the data.

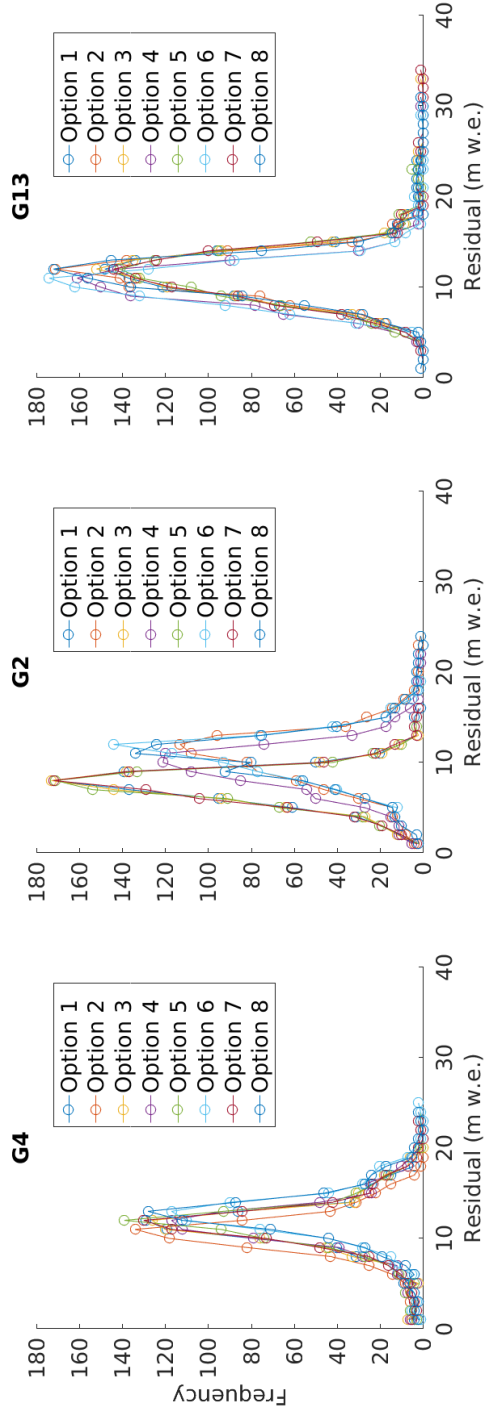


Figure 23: Residuals of SWE predicted using MLR for all options of estimating density.

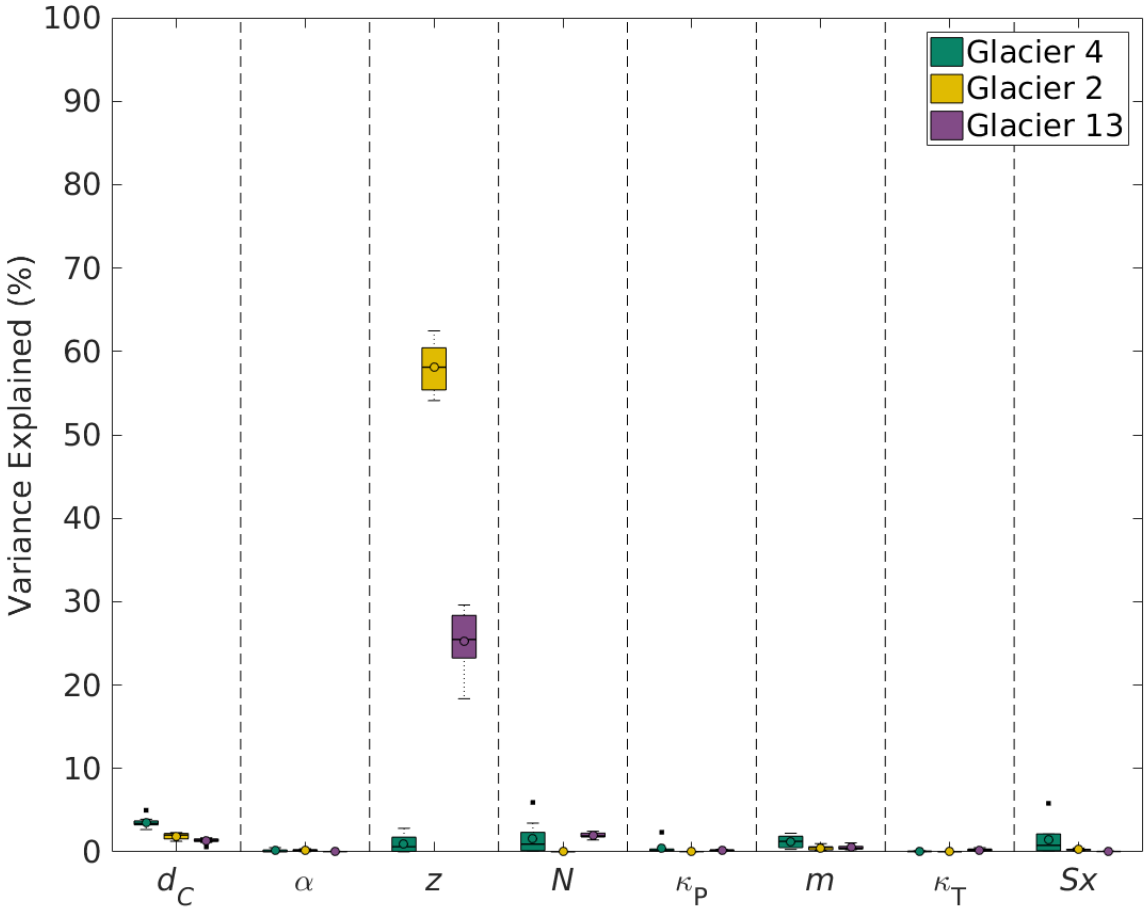


Figure 24: Boxplot showing the range of percent variance explained by each topographic parameter for each option of estimating snow water equivalent (SWE). Topographic parameters include aspect (α), elevation (Z), northness (N), profile curvature (κ_P), slope (m), tangent curvature (κ_T), wind redistribution (Sx) and distance from centreline (d_C).

2.2 Bayesian Model Averaging

2.2.1 Background

Bayesian model averaging (BMA) is a method of estimating all possible linear combinations of predictor variables and then averaging over all models (Raftery and others, 1997; Wasserman, 2000; Raftery and others, 2005). This method is based on Bayesian principals where we wish to determine the probability of an outcome based on an initial “guess” as well as the data provided. Given that the predictive outcome has a probability distribution of x given y , written as $P(x|y)$, we use Bayes’ rule to write this as

$$P(x|y) = \frac{P(y|x)P(x)}{P(y)}. \quad (20)$$

$P(x|y)$ is often called the posterior model probability (PMP). The quantity $P(y|x)$ is the likelihood function, which determines unknown parameters from a known outcome (i.e. observed data). The term $P(x)$ is an observer determined prior probability distribution (typically just called a *prior*) and it reflects the prior knowledge of the system (Raftery and others, 1997). Choosing an appropriate prior is one of the most challenge components of Bayesian probability theory (Wasserman, 2000). The $P(y)$ term can be obtained by integrating $P(y|x)P(x)$ over all x and is thus a constant for all models that is typically discarded (Wasserman, 2000).

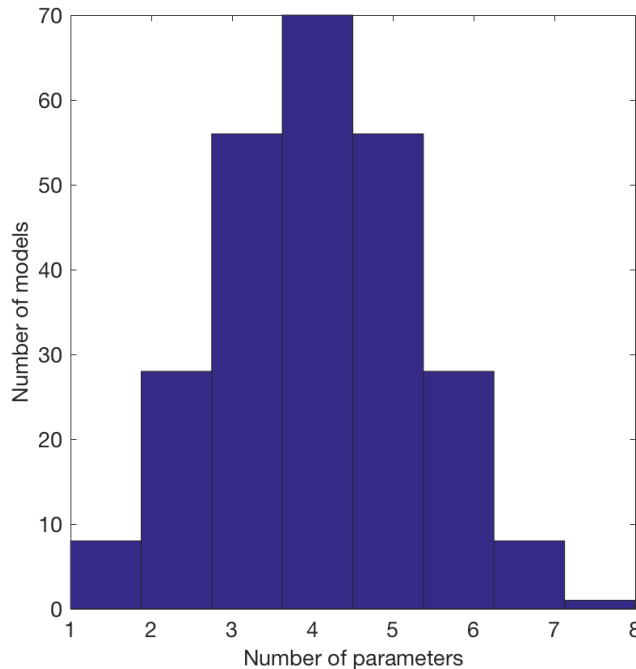


Figure 25: Uniform model prior for eight topographic regressors used in BMA.

little effect on the posterior. The final value of the desired output is often reported as the posterior distribution mean or the value that maximizes the log-likelihood.

Within BMA, Bayes' theorem is used to find the posterior model probability and this is used as a weight when averaging over all models (Wasserman, 2000). The model weighted posterior distribution for the coefficients β of k number of models after renormalization is given by

$$P(\beta | y, X) = \sum_{i=1}^{2^k} P(M_i | X, y) P(\beta | M_i, y, X), \quad (22)$$

where the responding variable is given by y and the matrix of variables is given by X (Raftery and others, 1997). Here, the model prior is $P(M_i | X, y)$ and the likelihood for the β coefficient is $P(\beta | M_i, y, X)$.

Together then, the posterior model probability is a function of both the model prior, specified by the researcher, as well as the distribution of the observed data — it is the transformation of the prior as a result of considering collected data (Wasserman, 2000). This can be loosely expressed as

$$\text{posterior} \propto \text{prior} \times \text{likelihood} \quad (21)$$

If the prior is uninformative then the posterior will be strongly influenced by the data (Wasserman, 2000). An informative prior will result in a posterior that is a mix of the prior and the data as as the prior becomes more informative, the amount of data needed to transform the distribution increases. If there is a large amount of data then the prior will have

There are a number of different priors to describe model size distribution that have been applied in BMA. A commonly used prior is the ‘uniform’ prior, which assumes a normal model distribution with a total of 2^n models, where n is the number of regressors (Wasserman, 2000). This model prior states that the observer has no knowledge of the system and all models are equally likely. The uniform prior has a prior model probability of the form $P(M_i) = 2^{-n}$, as shown in Figure 25, which is symmetric about the mean $n/2$ (Zeugner and Feldkircher, 2015). This prior inherently favours models of an intermediate size.

Other types of priors include those that are skewed to favour smaller models, ones with equal probability for all model sizes, and ones with varying probability for individual regressors. In this project, a uniform prior was chosen because there was no knowledge of what the model distribution would look like and to match the distribution of models sizes in the MLR analysis. This is commonly done in BMA (Wasserman, 2000).

With a small number of regressors, the posterior of all possible models can be determined. As the number of regressors increases, this computation becomes increasingly expensive since the total number of models is 2^n . To overcome this, BMA can use Markov chain Monte Carlo (MCMC) model composition to directly approximate the posterior distribution (Wasserman, 2000). In our study, there are eight regressors, resulting in $2^8 = 256$ models. It is possible to visit all models and to obtain an exact solution so an MCMC model composition was not employed.

BMA allows for the calculation of a metric called the posterior inclusion probability (PIP), which is used to evaluate the importance of a regressor in explaining the observed data. PIP is the sum of all posterior model probabilities (PMP) where the variable was included in the mode (Zeugner and Feldkircher, 2015). A higher PIP indicates that the regressor is more important in the regression.

2.2.2 Methods

The BMA process was implemented in R, using the Bayesian model statistics (BMS) package developed by Zeugner and Feldkircher (2015). The function `BMS.R()` computes the β coefficients for all topographic parameters for all study glaciers as well as the percent variance explained by each parameter using the following steps:

1. The SWE observations and associated topographic parameters are called in the function.
2. A portion of the data (2/3 as suggested by Kohavi and others (1995)) is randomly chosen as the calibration set and saved as a .mat file.
3. The R script is called through the terminal
 - (a) The R script imports the .mat file with SWE and topographic parameter values. It then creates a data frame with the SWE values as the first column and the topographic parameters as the remaining columns.
 - (b) The BMS package is used to complete BMA for the imported values. A uniform model prior was chosen. The mean coefficient value, coefficient standard devi-

ation, PIP, and the posterior probability of a positive coefficient (how probable it is for the sign of the coefficient to be positive) were computed.

- (c) The coefficients are saved as a .mat file.
4. Values calculated in R are loaded into Matlab and a data table is created with the coefficients.
5. The remaining portion of the topographic parameter values (1/4) are then used to calculate a modelled value of SWE at those locations. These are compared to the observed SWE values and a RMSE value is determined.
6. The above step are completed 1000 times and the coefficients associated with the lowest RMSE are chosen.
7. Percent variance explained by each parameter is the calculated in the same way as for the MLR (see Section 2.1.2).
8. The final table of values includes the coefficients and percent variance explained for all topographic parameters associated with the lowest RMSE. It also includes the intercept and the actual RMSE value. This table is returned from the function.
9. The residuals of the best BMA fit are also calculated and can be return from the function.

2.2.3 Results

The coefficients determined using BMA for density Option 8 can be seen in Table 4. These coefficients were found for standardized values of topographic parameters so their magnitude is indicative of their importance in predicting SWE. The range of percent variance explained by each variable (from all density options) can be seen in Figure 29. The fit between modelled SWE and observed SWE for each glacier for density option 8 can be seen in Figure 26 and the fit for all density options in Figure 27. The distribution of residuals in then plotted in Figure 28. A map of the predicted values of SWE over the entire glacier using density option 8 can be seen in Figure ??.

For Glacier 4, the largest coefficients are distance from centreline and slope, which are an order of magnitude larger than the remaining coefficients. Both coefficients are negative, which indicates less snow along the margins of the glacier and less on steeper slopes. These coefficients account for the largest percentage of variance explained, although this percentage is very small (< 3% each). The map of predicted SWE for the entire glacier closely resembles the distribution of distance from centreline (Figure 7), which also shows its dependence on this parameter. Overall, the modelled winter balance for Glacier 4 is very poorly explained by the topographic parameters, which results in no correlation between modelled and observed SWE ($R^2 = 0.05$). The modelled values of SWE are largely determined by the intercept value. RMSE???

For Glacier 2, the largest coefficient (by an order of magnitude) is elevation. This coefficient is positive, which means that SWE will increase with elevation. Elevation explains the largest amount of variance (52%) and this is consistent for all density options. The map of modelled SWE shows this strong dependence on elevation since the values closely resemble the elevation map (Figure 5). The second largest coefficient is distance from centreline, which accounts for 2% of the variance. Overall, the modelled winter balance is a good estimation of observed SWE ($R^2 = 0.62$) although it tends to underestimate the amount of accumulation.

For Glacier 13, the largest coefficient is elevation with distance from centreline and “northness” also of the same order of magnitude. All three coefficients are positive, which means that cells at higher elevation, closer to the margins, and more north facing had higher amounts of SWE. Elevation explains the majority of the variance (23%), while distance from centreline and “northness” explain far less (<2% each). The map of modelled SWE displays an increase with elevation, although it is not strong, especially considering the large range of elevation on this glacier. Overall, the MLR modelled winter balance is poorly related to observed SWE ($R^2 = 0.34$) and tends to underestimate the amount of accumulation.

Qualitatively, there is little variation in the fit between modelled and observed winter balance between the various density options for all glaciers and the residuals display a similar distribution between the density options. The percent variance explained by each parameter also varies little between different density options.

Table 4: BMS coefficients for topographic regression between measured SWE and standardized topographic parameters that include distance from centreline (d_C), elevation (z), aspect (α), slope (m), northness (N), profile curvature (κ_P), tangent curvature (κ_T), and wind redistribution (Sx). Since parameters are standardizes, the magnitude of the coefficients is representative of their importance in predicting SWE. The root-mean-squared error (RMSE) between modelled SWE using those coefficients and observed SWE is also given.

	Glacier 4	Glacier 2	Glacier 13
d_C	-0.028	0.021	0.015
z	<0.001	0.118	0.051
α	-0.001	-0.001	0.001
m	-0.014	0.002	-0.004
N	<0.001	<0.001	0.014
κ_P	0.001	<0.001	-0.001
κ_T	<0.001	<0.001	-0.002
Sx	0.002	<0.001	<0.001
Intercept	0.623	0.266	0.242
RMSE			

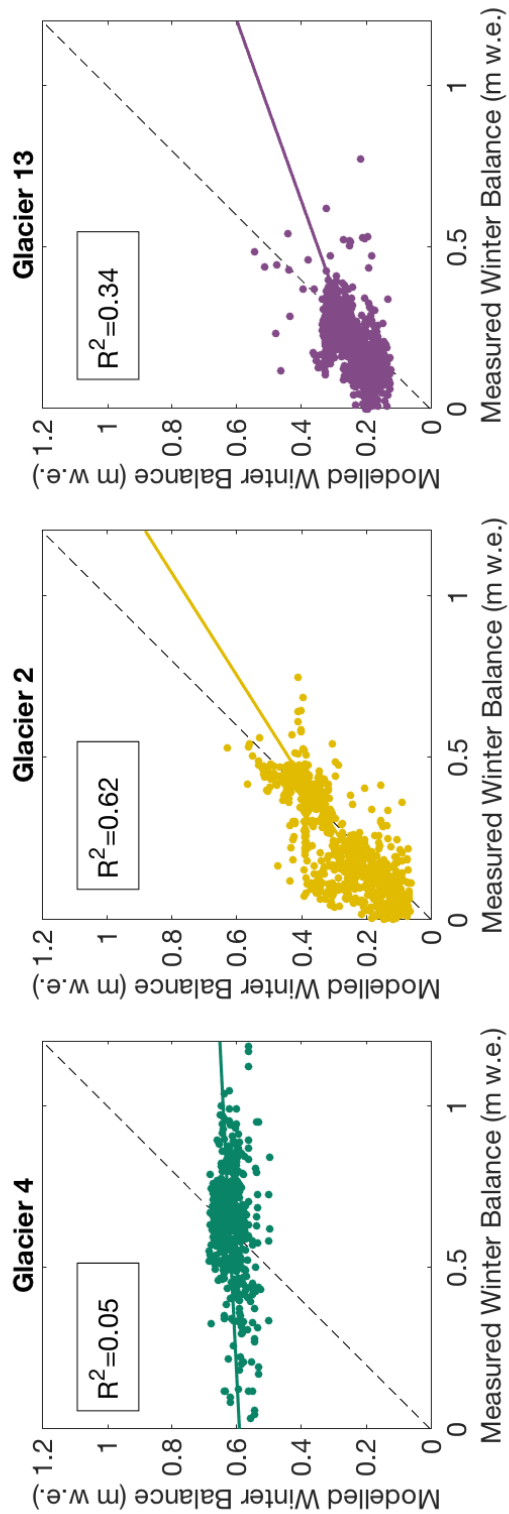


Figure 26: Comparison of predicted (BMA) and observed (original) snow water equivalent (SWE) for three study glaciers. The SWE values were calculated inverse distance weighted snowpit densities (Option 8).

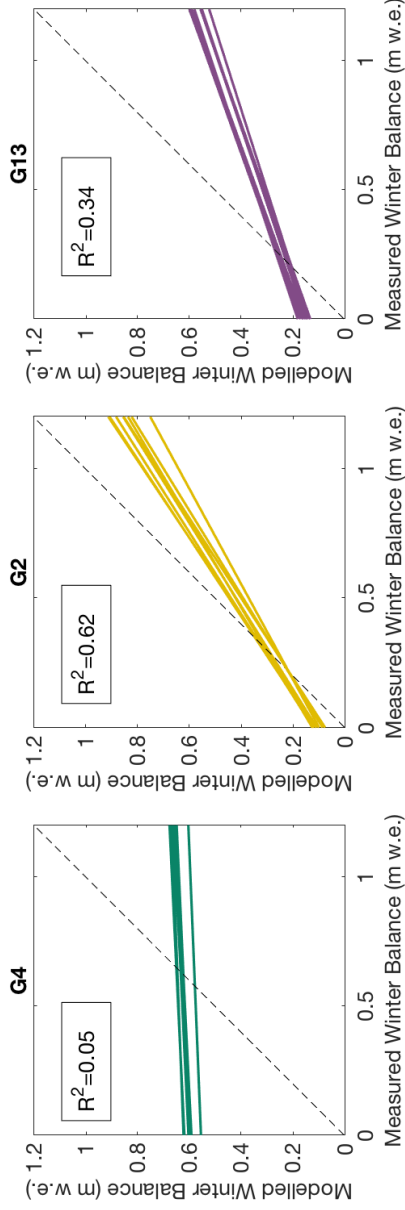


Figure 27: Plot of all linear fits between modelled (BMA) and observed SWE using eight options for calculating density. Mean R^2 value is shown for each sub-plot and a reference 1:1 line is also provided. See Figure 26 for a plot of the data.

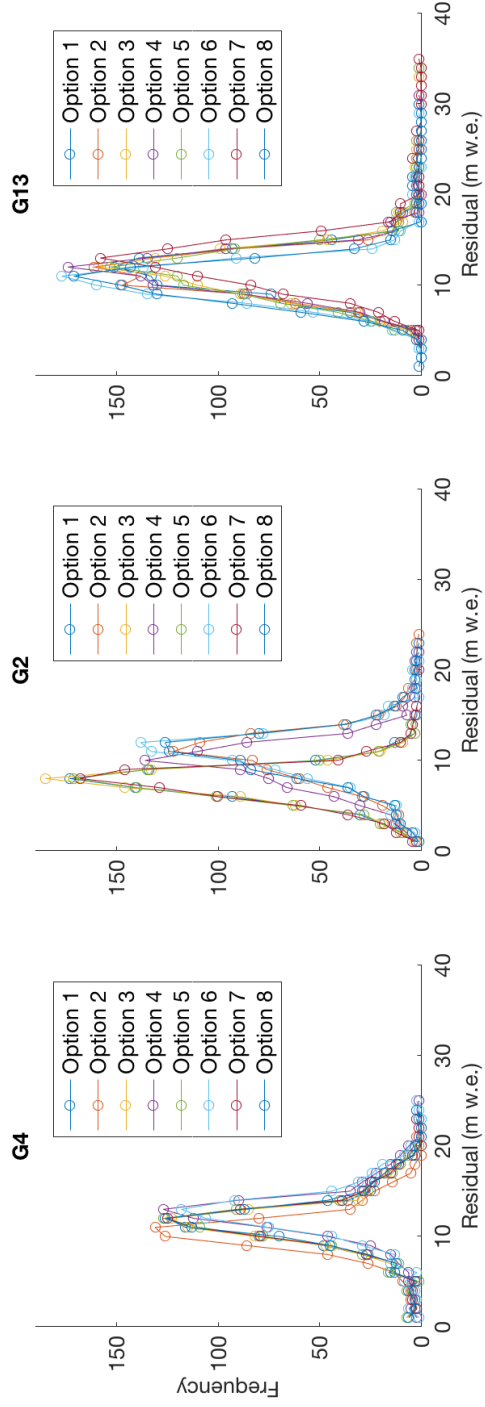


Figure 28: Residuals of SWE predicted using BMA for all options of estimating density.

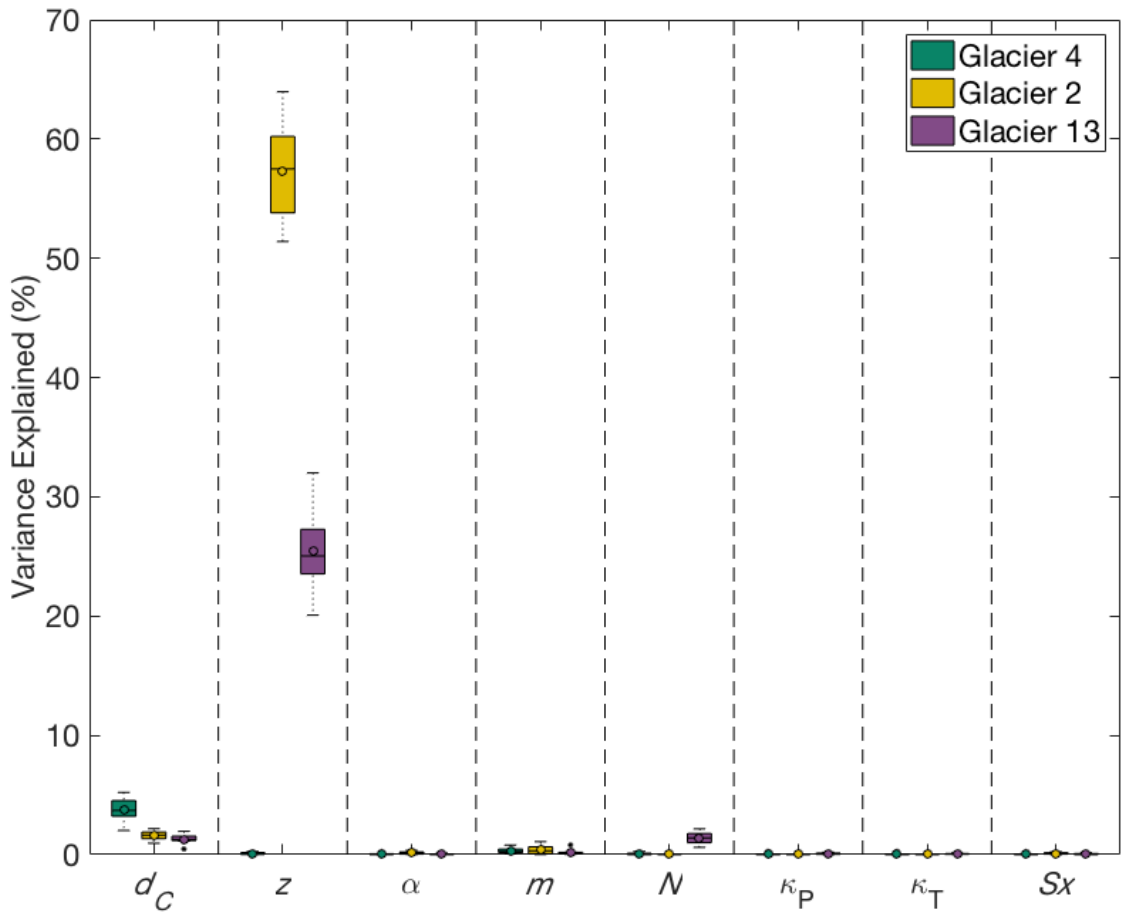


Figure 29: Boxplot showing the range of percent variance explained by each topographic parameter as calculated using BMA for each option of estimating snow water equivalent (SWE). Topographic parameters include aspect (α), elevation (z), northness (N), profile curvature (κ_P), slope (m), tangent curvature (κ_T), wind redistribution (Sx) and distance from centreline (d_C).

2.3 MLR and BMS comparison

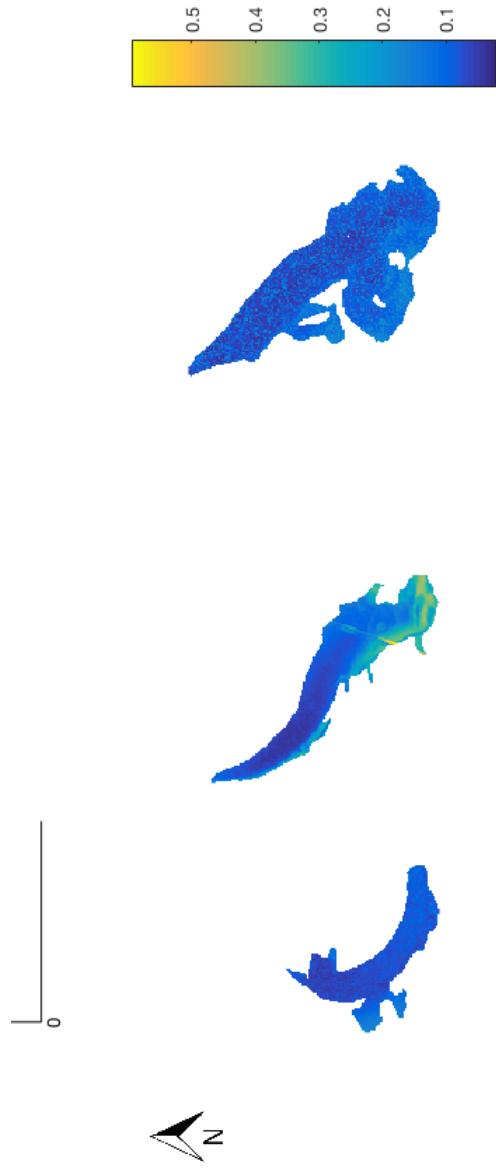


Figure 30: Map of the difference between maximum and minimum SWE values for each DEM cell between all density options and from both MLR and BMA.

References

- Basist A, Bell GD and Meentemeyer V (1994) Statistical relationships between topography and precipitation patterns. *Journal of climate*, **7**(9), 1305–1315 (doi: 10.1175/1520-0442(1994)007<1305:SRBTAP>2.0.CO;2)
- Berthier E, Arnaud Y, Kumar R, Ahmad S, Wagnon P and Chevallier P (2007) Remote sensing estimates of glacier mass balances in the Himachal Pradesh (Western Himalaya, India). *Remote Sensing of Environment*, **108**(3), 327–338
- Berthier E, Schiefer E, Clarke GK, Menounos B and Rémy F (2010) Contribution of Alaskan glaciers to sea-level rise derived from satellite imagery. *Nature Geoscience*, **3**(2), 92–95
- Burnham KP and Anderson DR (2004) Multimodel Inference: Understanding AIC and BIC in Model Selection. *Sociological Methods & Research*, **33**(2), 261–304 (doi: 10.1177/0049124104268644)
- Cohen J, Cohen P, West SG and Aiken LS (2013) *Applied multiple regression/correlation analysis for the behavioral sciences*. Routledge
- Davis JC and Sampson RJ (1986) *Statistics and data analysis in geology*, volume 646. Wiley New York et al.
- Hofierka J, Mitášová H and Neteler M (2009) Geomorphometry in GRASS GIS. *Developments in Soil Science*, **33**, 387–410 (doi: 10.1016/S0166-2481(08)00017-2)
- Horn BK (1981) Hill shading and the reflectance map. *Proceedings of the IEEE*, **69**(1), 14–47 (doi: 10.1109/PROC.1981.11918)
- Kohavi R and others (1995) A study of cross-validation and bootstrap for accuracy estimation and model selection. In *Ijcai*, volume 14, 1137–1145
- Korona J, Berthier E, Bernard M, Rémy F and Thouvenot E (2009) SPIRIT. SPOT 5 stereoscopic survey of Polar Ice: reference images and topographies during the fourth International Polar Year (2007–2009). *ISPRS Journal of Photogrammetry and Remote Sensing*, **64**(2), 204–212
- McGrath D, Sass L, O’Neel S, Arendt A, Wolken G, Gusmeroli A, Kienholz C and McNeil C (2015) End-of-winter snow depth variability on glaciers in Alaska. *Journal of Geophysical Research: Earth Surface*, **120**(8), 1530–1550 (doi: 10.1002/2015JF003539)
- Mitášová H and Hofierka J (1993) Interpolation by regularized spline with tension: II. Application to terrain modeling and surface geometry analysis. *Mathematical Geology*, **25**(6), 657–669 (doi: 10.1007/BF00893172)

- Molotch N, Colee M, Bales R and Dozier J (2005) Estimating the spatial distribution of snow water equivalent in an alpine basin using binary regression tree models: the impact of digital elevation data and independent variable selection. *Hydrological Processes*, **19**(7), 1459–1479 (doi: 10.1002/hyp.5586)
- Neteler M and Mitášová H (2013) *Open source GIS: a GRASS GIS approach*, volume 689. Springer Science & Business Media
- Olaya V (2009) Basic land-surface parameters. *Developments in Soil Science*, **33**, 141–169
- Raftery AE, Madigan D and Hoeting JA (1997) Bayesian Model Averaging for Linear Regression Models. *Journal of the American Statistical Association*, **92**(437), 179–191 (doi: 10.1080/01621459.1997.10473615)
- Raftery AE, Gneiting T, Balabdaoui F and Polakowski M (2005) Using Bayesian Model Averaging to Calibrate Forecast Ensembles. *Monthly Weather Review*, **133**(5), 1155–1174 (doi: 10.1175/MWR2906.1)
- Revuelto J, López-Moreno JI, Azorín-Molina C and Vicente Serrano SM (2014) Topographic control of snowpack distribution in a small catchment in the central Spanish Pyrenees: intra-and inter-annual persistence (doi: 10.5194/tc-8-1989-2014)
- Wasserman L (2000) Bayesian Model Selection and Model Averaging. *Journal of Mathematical Psychology*, **44**(1), 92–107, ISSN 0022-2496 (doi: 10.1006/jmps.1999.1278)
- Winstral A, Elder K and Davis RE (2002) Spatial snow modeling of wind-redistributed snow using terrain-based parameters. *Journal of Hydrometeorology*, **3**(5), 524–538
- Woo MK and Marsh P (1978) Analysis of Error in the Determination of Snow Storage for Small High Arctic Basins. *Journal of Applied Meteorology*, **17**(10), 1537–1541 (doi: 10.1175/1520-0450(1978)017<1537:AOEITD>2.0.CO;2)
- Zeugner S and Feldkircher M (2015) Bayesian Model Averaging Employing Fixed and Flexible Priors: The BMS Package for R. *Journal of Statistical Software*, **68**(4), 1–37